Title

Effects of the c-Si/a-SiO 2 interfacial atomic structure on its band alignment: an ab initio study

Journal

Physical Chemistry Chemical Physics, 19(48)

ISSN

0956-5000

Authors

Zheng, Fan

Pham, Hieu H

Wang, Lin-Wang

Publication Date

2017-12-13

DOI

10.1039/c7cp05879a

Peer reviewed

The effects of c-Si/a-SiO_2 interface atomic structure on its band alignment: an *ab initio* study

Fan Zheng,[1] Hieu H. Pham,[1] and Lin-Wang Wang[1]

[1] *Joint Center for Artificial Photosynthesis and Materials Sciences Division, Lawrence Berkeley National Laboratory, Berkeley, California 94720, USA.*

The crystalline-Si/amorphous-SiO_2 (c-Si/a-SiO_2) interface is an important system used in many applications, ranging from transistor to solar cell. The transition region of the c-Si/a-SiO_2 interface plays a critical role in determining the band alignment between this two regions. However, the question of how this interface band offset would be affected by the transition region thickness and its local atomic arrangement, has yet fully investigated. Here, by controlling the parameters of the classical Monte-Carlo bond switching algorithm, we have generated the atomic structures of the interfaces with various thickness, as well as containing Si at different oxidation states. Hybrid functional method, as shown by our calculations to reproduce the *GW* and experimental results for bulk Si and SiO_2, are used to calculate the electronic structure of the heterojunction. This allows us to study the correlation between the interface band characterization and its atomic structures. We find that although the systems with different thickness show quite different atomic structure near the transition region, the calculated band offset tends to be the same, unaffected by the detail interfacial structure. It is shown that our band offset calculation agrees well with the experimental measurements. This robustness of the interface electronic structure to its interfacial atomic details could be another reason for the success of the c-Si/a-SiO_2 interface in Si based electronics applications. Nevertheless, when the reactive force field is used to generate the a-SiO_2 and the c-Si/a-SiO_2 interface, the band offset significantly deviates from the experimental values by about 1 eV.

I. INTRODUCTION

Amorphous oxides are often used as insulating, protection or carrier stopping layers for many electronic and optoelectronic applications. In such applications, the electronic structure of the system, e.g., the band alignment between the oxides and the underlying crystal substrate, as well as possible interface electronic states, are of high interest. Although density functional theory (DFT) interface studies become quite common, and they are often complemented by high level methods (like GW) band gap corrections, it is still relatively rare to find theoretical amorphous-crystal interface studies. This does not mean the crystal/amorphous interface is not important, quite the contrary, such interfaces exist in majority of electronic applications. The main reason for the lack of theoretical study is the difficulty to construct the reliable atomic structure of the interface, and to test such structures against experiment once structure is constructed. Furthermore, unlike the crystal/crystal interface, the crystal/amorphous interface often requires large supercells, which makes the calculation much more expensive. However, with the advance in computer power and computational algorithm, we can now calculate systems consisted with a few hundred atoms, and use methods like the hybrid functional which has a potential to describe the electronic structure more accurately than the local or semilocal functionals such as local density approximation (LDA) or generalized gradient approximations (GGA). On the other hand, the new applications of the amorphous oxide insulating or protection layer, e.g., in solar cell or solar electric chemical cell, and the push for a more fundamental understanding of their carrier dynamics, raise renewed interest of these systems. In this work, we use c-Si/a-SiO_2 as an example to study such crystal/amorphous interface. In particular, we like to compare different interfacial atomic structures and their electronic structure consequences. From such a comparative study, we can estimate both the reliability of the different procedures to construct the atomic structure, as well as the physical understanding of different interfaces.

c-Si/a-SiO_2 interface is ubiquitous in Si based electronic devices. It is one of the most well studied crystal-amorphous interface due to its predominance in electronic applications[1–16] . Besides in the CMOS technology it is also widely used in other applications. For example, in photoelectrochemistry, the amorphous SiO_2 has been one of the most popular protection layers to protect the light absorber, such as Si from being corroded by the electrolyte or water[17]. Current engineering technique can tune the thickness of SiO_2 film to as small as 0.6 nm, in order to improve the the gate capacitance in the metal-oxide-semiconductor capacitor, or to enhance the hole tunneling transport in silicon photoanode[18]. With such thin SiO_2, the details of the interface with Si becomes

extremely important. Different synthesizing and oxidation procedures might produce different interfacial atomic structure. Understanding the influence of the interfacial atomic structure to the electronic structure of system is therefore of great significance. In late 1980's, there were a burst of theoretical studies for c-Si/a-SiO_2. These studies have yielded band offsets in agreement with the experiments. But most of those studies are based on relatively small supercell systems in particular for *ab initio* calculations. Often, only one atomic structure is used, and there was no systematic comparison for different atomic structures. Moreover, most previous theoretical studies are based on LDA/GGA, with estimated postprocessing corrections to the LDA/GGA band gap error. In the current work, we use different strategies to construct the crystal/amorphous interface, and compare different interfacial atomic structures. We also use hybrid functional (HSE) to directly calculate the whole system without the need for further postprocessing corrections.

It is well known from early studies, one predominant feature of the c-Si/a-SiO_2 interface is its relative abruptness in the interfacial layers, as shown in TEM images[17]. Nevertheless, the interface can extend beyond one monolayers, to two or three atomic monolayers.[19–22] Even a more extensive transition layer larger than 10 Å has been identified using X-rays[8,23]. Within the transition region, photoemission and photoelectron spectroscopies demonstrate the presence of the suboxide layer[20,21,24], comprised of Si with oxidation states as Si^{+1}, Si^{+2} and Si^{+3}. Further measurements show their ratio to be 1:2:3 or 1:2:1 depending on synthesizing conditions[25,26]. Meanwhile, molecular dynamics (MD) using reactive force field[5,27] and Monte-Carlo (MC)[28] simulations have also shown the existence of beyond 10 Å interfacial layer. Owing to their relatively small computational costs, different valence force fields have been used to study both bulk a-SiO_2 and its interface with Si[29,30]. The band gap and band offset were mainly computed using LDA or GGA method. However, the LDA/GGA methods do not always show agreement with the experimentally measured band offset due to the well-known issue of the band-gap underestimation. As a result, further corrections such as *GW* and hybrid functional have been used to correct the LDA/GGA band gaps, showing good agreement with the experiments[31–33]. But as far as we know, there were no systematic study of electronic structures of different interfacial atomic structures, in particular using electronic structure calculation methods (e.g., the hybrid exchange-correlation functional) without postprocessing corrections directly.

As illustrated in both experimental and theoretical work, the size of the transition regions spans a broad range. As a result, the thickness of the interface is non-negligible when compared to the thickness of the SiO_2 layer for the thin SiO_2 layer applications. Therefore, understanding the effect of the transition region to the electronic structure of the interface is of great interest. In this

study, via the bond switching (BS) MC simulations, the thickness of the transition region will be measured by the maximum number of Si atoms connected via continued Si–Si bonds starting from the fixed crystal Si region. The band offset is computed using the hybrid functional methods. A special technique is developed which allows the application of a regional mixing parameter to the hybrid functional, hence able to describe the band gaps of both Si and SiO_2 regions accurately. Our results show excellent agreement with the experimental band offset, and also reveal a robustness of the band offset to the detail interfacial atomic profile.

II. CALCULATION METHODS

A. Monte-Carlo simulation

The continuous random network, or say the BS MC simulation, has been demonstrated to be an effective way to generate the amorphous structures for covalent bonding materials.[34–37] During the BS procedure, a pair of nearby bonds, (either Si–Si or Si–O type bonds) are selected. This pair of bonds: A–B, C–D, are switched into a new pair of bonds: A–C, B–D. By enforcing the new bond topology into valence force field (VFF), the switched atomic structure is fully relaxed. The total energy of the relaxed structure is compared with the previous step, and this new structure is accepted or rejected following the Metropolis MC scheme. Many sophisticated force fields such as Tersoff and its derivatives[38–41], Yasukawa[42], and Stillinger-Weber[43] potentials were applied to the studies of the Si/SiO_2 interface. However, many of such force fields are designed to break the bond, which does not apply to the continuous random network scheme. VFF as the simplest one is capable of describing the structure well, and it is straightforward to implement it into the BS MC scheme. In our simulation, the following VFF[44] is used to relax the structure.

$$E_{\text{tot}} = \frac{1}{2}\sum_i k_b(d_i - d_0)^2 + \frac{1}{2}\sum_{i,j} k_\theta(c_{ij} - c_0)^2 + U_{\text{repulsion}} \tag{1}$$

where $k_{b,\text{Si-O}} = 27$ eV/Å^2, $k_{b,\text{Si-Si}} = 9.08$ eV/Å^2, $k_{\theta,\text{Si-O-Si}} = 0.75$ eV, $k_{\theta,\text{O-Si-O}} = 4.32$ eV, $k_{\theta,\text{Si-Si-Si}} = 3.58$ eV, and $k_{\theta,\text{Si-Si-O}} = (k_{\theta,\text{Si-Si-Si}} k_{\theta,\text{O-Si-O}})^{\frac{1}{2}}$ eV, d_0 and c_0 are taken from the DFT relaxed Si and SiO_2. The last term $U_{\text{repulsion}} = \frac{1}{2}\sum_{\langle i,j\rangle} k_r(d_{ij} - d_{\text{neighbor}})^4$ when $d_{ij} < d_{\text{neighbor}}$ is to avoid the overlap of two atoms which are not directly connected by a bond. k_r is set to be 1 eV/Å^4. d_{neighbor} is taken differently depending on the two neighboring atomic species ($d_{\text{neighbor,Si-O}} = 3.2$Å, $d_{\text{neighbor,O-O}} = 2.58$Å, $d_{\text{neighbor,Si-Si}} = 3.84$Å). This term turns out to

be important to obtain reasonable structure, in particular near the interface[29,30,34]. By taking derivative of the total energy to the atomic position, the force can be derived. With the total energy and the force as the inputs, the conjugate-gradient minimization scheme is used to relax the structure. Since the MC is used to obtain the bond topology for the amorphous structure, the accuracy of the relaxation is not crucial, and we set the force threshold to be 0.3 eV/Å.

The middle three layers of Si and their bonds are fixed in order to maintain the crystalline structure of Si (Fig. 1). However, if all other Si atoms are allowed to participate in the bond switch, it is easy to form the Si–Si bonds extended to the SiO_2 regions. These Si–Si bonds cause suboxide layers with Si^{+1}, Si^{2+},Si^{3+} oxidation states. In order to quantify the thickness of this suboxide layer, we count the maximum number (n) of Si atoms connected via the continued Si–Si bonds starting from the fixed Si atom layer (Fig. 1). In our BS MC procedure, we deliberately limit n to be 2, 3 and 4 (e.g., to make a $n = 3$ suboxide layer, if n is larger than 3 during MC, the bond switch will be rejected) to generate different interfacial thickness. This allows us to have a systematic procedure to produce and thoroughly study different transition layers at various thicknesses. Here, n=2 corresponds to the "abrupt" interface with only one layer of atoms for the transition region, which has two Si–O bonds and two Si–Si bonds. Such abrupt interface is interesting since that is the case for most c-Si/c-SiO_2 interface constructed in many theoretical studies. It is interesting to note that it is possible to have such interface in the c-Si/a-SiO_2 interface structure. During the MC simulation, following previous literatures, the first $N/2$ steps BS steps are all accepted to fully amorphize the crystal at the beginning. Then, the stimulated annealing from very high temperature (10000K) is used to cool the structure and reduce the local strain. During the temperature cooling, a new temperature is set as 70% of the previous temperature step, and a total of around 300 thousand BS MC steps are performed to reach the equilibrium.

B. Reactive force field MD

We have also used MD simulation and "melt-and-quench" technique to obtain the c-Si/a-SiO_2 along [001] direction using reactive force field (ReaxFF)[45] approach. More specifically, the interatomic interactions between Si–Si, Si–O and O–O pairs are characterized using the ReaxFF, which has been shown to reproduce well the structural properties of crystalline SiO_2. During the molecular dynamics simulation, the Si part is kept frozen and the SiO_2 part was firstly heated up to high temperature until the crystals completely lose their structural memory. This is then equilibrated for a short period at this temperature (for 5 ps at 3500 K), followed by slowly cooling to room

temperature over 100 ps, which allows the formation of the SiO_2 amorphous phase. The time step for the MD simulations is 0.5 fs and the canonical ensemble (NVT, constant volume and constant temperature) was used. Here we followed the same procedure as employed by Kovacevic *et al* in our MD simulation details.[46]

C. Electronic structure calculation

The plane-wave package PWmat[47,48] is used to relax the DFT atomic structure and compute the electronic properties, using GGA exchange-correlation functional[49]. The PWmat produces essentially the same results as that of Quantum Espresso[50], but with efficient GPU accelerations. The norm-conversing pseudopotential is used with a wavefunction energy cutoff of 50 Ryd with single Γ k-point[51]. In order to obtain the band offset, the last few snapshots from the end of the MC simulation are fully relaxed using DFT until all the components of the forces are below 0.05 eV/Å. The local density of states are then computed to reveal the layer-resolved band energies along the direction perpendicular to the interface in order to illustrate the band offset.

However, such band offset obtained from GGA suffers from the underestimation of the band gap. Hybrid functional which includes the exact exchange integral has been shown to improve both the band gaps of bulk materials as well as the band offsets of the heterostructures[52]. Furthermore, the amount of exact exchange represented by a mixing parameter α, is inversely proportional to the high frequency dielectric constant of the material (ϵ_∞)[53]. Thus, in theory, the mixing parameter for small band gap Si and the large band gap SiO_2 should be different. Indeed, this is true in practice. In our PWmat calculation using the norm conserving pseudopotentials, we found that a mixing parameter of 0.15 is needed for crystal Si and 0.35 is needed for crystal SiO_2 in order to yield their perspective band gaps of 1.12 and 8.5 eV. To solve this problem, we have introduced an atomic specific mixing parameter. More specifically, an atom-weighted mask function $f(\mathbf{r}) = 1+\sum_i a_i \mathrm{e}^{-(\mathbf{r}-\mathbf{R_i})^2/\sigma^2}$ is introduced with a_i being atomic specific parameter for atom i, and R_i is the atomic position. Then the exchange interaction in the total energy expression can be written as: $\sum_{i,j} 0.25 o(i) o(j) \int\int \psi_i(\mathbf{r})\psi_j^*(\mathbf{r}) f(r) \frac{\mathrm{erfc}(\omega(\mathbf{r}-\mathbf{r}'))}{|\mathbf{r}-\mathbf{r}'|} f(r')\psi_i^*(\mathbf{r}')\psi_j(\mathbf{r}') d^3\mathbf{r} d^3\mathbf{r}'$, here $\psi_i(\mathbf{r})$ are wave functions, and $o(i)$ is its occupation number. The prefactor 0.25 is the original mixing parameter in the HSE. The local part of the GGA exchange energy density will also been modified by a factor of $1 - 0.25 f(r)^2$. By setting a_i for each atom type, an effective local mixing parameters can be achieved. We have determined the a_i parameters by requiring the hybrid functional to reproduce the experimental crystal Si and bulk amorphous SiO_2 band gaps as $a_{\mathrm{Si,Silicon}} = -0.1$,

$a_{Si,O;SiO_2} = 0.24$. As we will demonstrate below, by implementing this method, the appropriate band offset can be obtained through a self-consistent hybrid functional calculation, which should provide more reliable electronic structures and wave function localizations than postprocessing corrections. Here, all the HSE calculations are done with the PWmat code, which has a fast scheme to calculate the HSE. For our 513 atom supercell system, with 2592 electron and 50 Ryd energy cutoff, the self-consistent HSE calculation takes about 4 hours using eight GPUs.

III. RESULTS AND DISCUSSIONS

A. Structure of the interface

To validate the effectiveness of the VFF and the BS MC method, we test our procedure by first building the amorphous bulk SiO_2 with 243 atoms. Shown in Fig. 2 is the calculated radial distribution functions (RDF) for the systems prepared by BS MC and ReaxFF MD, compared with the experimental values[54]. From this graph, we can see that the BS MC method reproduces not only the peaks for short-range radius but also the main peaks for distance larger than 5 Å, demonstrating its validity in describing the amorphous feature of SiO_2. For ReaxFF MD, although it predicts the first peak (Si–O bond) correctly, it deviates significantly from the experimental measured second peak (O–O distance), which may be caused by the lack of accuracy for the O–Si–O angle description. This can be further shown in Fig. 2b where the O–Si–O angle distributions of BS MC and ReaxFF MD amorphized structures are compared. As expected, most of the angles from BS MC simulation are around 109.5°, corresponding to the tetragonal cage of Si and O. However, the angles of the structure from the ReaxFF MD sample a broad range from 87° to 143°. In particular, the small angles around 90° correspond to a significantly underestimated value (~2.3Å) for O–O distance in the RDF.

With this confidence, we continue to explore the c-Si/a-SiO_2 interface using the BS MC simulation. The initial structure is constructed by stacking the crystalline SiO_2 on Si along [001] direction albeit with significant strain on the crystalline SiO_2. Here, the supercell 3×3×2 of the cubic Si is used for the Si part of the interface with a and b-axis fixed to be the lattice constant of the Si crystal. The length of the c axis of the supercell is determined based on the experimental density of amorphous SiO_2[29,55]. This initial structure is fully relaxed to relief the local strain at the interface with its resulting configuration as our initial atomic structure of the BS MC algorithm. It is followed by the BS MC with the procedure to control the interface thickness described above.

The last few snapshots from the MC simulations are used for DFT relaxations, and the resulting structures with different thickness of the transition regions are obtained and shown in Fig. 1. For all the structures with different interface thickness n, the SiO_2 part has been fully amorphized. When n=2, there is only a single atomic layer in the transition region, which mainly contains Si^{+2} atoms. As n increases to 3 and 4, we notice the continued Si–Si bonds spreading into the SiO_2 part (Fig. 1), forming all the five oxidation states of Si. In the mean while the number of layers containing suboxide Si atoms increases from monolayer to several atomic layers, expanding the transition regions.

Such expansion of the transition region can be further indicated by the characterization of the suboxide Si with its oxidation state determined by the number of the bonded oxygen atoms. Shown in Fig. 3 is the distribution of the oxidation states of Si along [001] direction under different thickness n. While, Si only shows 0 and +4 oxidation states deep inside Si and SiO_2 regions, suboxide Si becomes dominant near the interface. For example, the $n = 2$ structure shows the thinnest transition region, which occupies only single atomic layer (around 3Å). As n increases to 3 and 4, the transition region spans more layers, extending up to 5Å and 8Å, respectively. Furthermore, the ratio of these suboxide Si can be counted. In the case of $n = 2$, the ratio of states +1, +2 and +3 is distributed as 0:1:0 across the transition region. For $n = 3$ and $n = 4$, this ratio turns out to be 1:1.08:0.84 and 1:0.74:0.66, respectively. We see that the thicker interface has a more variety of Si valence states. The reported experimental value of this ratio varies widely, e.g. 1:2:3 in Ref.25, 1:2:1 in Ref.26 This might depend sensitively on the synthesis conditions or the experimental probing techniques. At this point, it is difficult to make a quantitative comparison with any specific experiments. We find that the valence states of Si is in roughly similar orders between +1, +2 and +3 states in n=3 and 4 interfaces. Thus these experimental interface might not be the abrupt interface as illustrated in n=2 case.

B. Electronic structure

The band gap of interface is controlled by the band gap of Si part, which is around 1.1 eV. Taking $n = 2$ structure as an example, shown in Fig. 4 is the local density of states (LDOS) summed for the Si crystal part (Si^0), amorphous SiO_2 part (Si^{+4} and O) and the transition part (Si^{+2}), calculated using the local parameterized HSE functional. As shown from the density of states, the states near the band gap are dominant by the Si atoms inside the Si layer, without any defect states in the band gap. To show this more clearly, we plot the wavefunction in real space for

the conduction band minimum (CBM) and valence band maximum (VBM) as illustrated in Fig. 4 b and c. It clearly shows that the wavefunctions are well localized inside the crystal Si. As for the Si^{+2} atoms in the transitional region, although they form only one atomic layer, their energies spread broadly for both low energy near the band gap (Si-like) and high energy away from the band gap (SiO_2-like). This may be owing to their mutual bonds with Si and O atoms. However, the energies of the Si^{+4} atoms are pushed far away from the band gap by Si–O bonding, featuring the SiO_2-like band energies.

The calculated LDOS is also used to estimated the "local" electronic structure and the band offset of the c-Si/a-SiO_2 interface. This is performed by averaging over the LDOS of the atoms within a given distance range along the [001] direction. Fig. 5a illustrates the GGA computed energies of CBM and VBM along the [001] direction for the n=2, 3 and 4 structures. The valence and conduction band offset (VBO and CBO) can be computed from the energy difference between the SiO_2 and Si parts, i.e. $\mathrm{VBO} = \mathrm{Max}\left[\mathrm{VBM_{Si}} - \mathrm{VBM_{SiO2}}\right]$ and $\mathrm{CBO} = \mathrm{Max}\left[\mathrm{CBM_{SiO2}} - \mathrm{CBM_{Si}}\right]$. For all the structures with different n we calculated, the CBO are around 1.8 eV, and the VBO are 2.5 eV, consistent with the other theoretical work[7,52].

Our results in Fig. 5 is a bit counter intuitive. For the n=2,3,4 cases, the amount of fixed bulk Si regions are the same. Intuitively, one expects the band offset starts at the same place from the bulk Si edge, and the thicker interfacial layer case of $n = 4$ should have a wider band offset turn-on region, just as the Si oxidation profile shown in Fig. 3. However, Fig. 5 shows that the band edge transition areas for n =2,3,4 have similar thickness (sharpness). Furthermore, the bulk Si like band edge has been pushed out for the $n = 4$ case from the structurally bulk Si region. As a result, the effective bulk SiO_2 region for the $n = 4$ case is much shorter, while the electronic transition areas measured from LDOS are the same for n =2,3,4. This will have significant consequence for the insulating capability and tunneling transport for the $n = 4$ case, particularly when the SiO_2 layer is thin. The reason for the push out of the Si bulk state into the transition area is that, whenever there are Si–Si bond, linking directly from the bulk Si area, the CBM and VBM wave function will be extended to those Si atoms, even though these Si atoms are already partially oxides as they also form Si–O bonds. This can be directly visualized from the real space wavefunctions for the band edges. Shown in Fig. 5b and c are the wavefunction for CBM and VBM of the n=3 and 4 structures. Together with the n=2 case (Fig. 4b), these Si atoms in the SiO_2 part though partially oxidized, still contribute to the band edge states. Also due to this contribution, as well as local strains caused by the thicker interface, the VBM and VBM wavefunction isosurfaces look more disordered in Fig. 5b and c even in the region of c-Si for n=3,4, compared to the case of n=2

shown in Fig. 4b and c.

The second significant finding of our simulation is that the magnitudes of the band offsets are independent of the interfacial transition layer thickness. As shown from this graph (Fig. 5), the thickness of the transition region does not affect the value of the band offset significantly. Different n, although show quite different "local" band gaps near the transition region, the overall band offset is still determined by the states inside the Si and SiO_2 parts, unrelated to the details of the transition region. This means the band offset is not driven by an interfacial dipole moment, since such dipole moment should depend on the details of the transition layer. Instead, the intrinsic band positions of bulk Si and SiO_2 determine the band alignment. It is possible the random nature of the amorphous structure allows the system to avoid the large interfacial dipole moment. It remains to be seen if this is generally true to crystal/amorphous band alignment.

As mentioned above, the different mixing parameter α can be assigned to atoms locally. In order to obtain the appropriate α for Si and SiO_2, we evaluate the band gaps calculated by different α for crystalline Si and amorphous SiO_2 shown in Fig. 6 a and b, respectively. For the amorphous SiO_2, a 243-atom bulk structure ($3 \times 3 \times 3$ supercell) is used, generated by the same BS MC simulation procedure and relaxed by GGA, which is large enough to represent the SiO_2 part in the interface. From the linear relation of the band gap and a_i, the value of the a_i can be easily obtained to reproduce the experimental band gap. We choose a_i = -0.1 for Si at pure Si region, and 0.24 for Si and O in amorphous SiO_2 region. We employ this newly developed hybrid functional calculation method and compute the band offsets as shown in Fig. 6 c for the structures with n=2, 3 and 4. From this graph, the HSE-calculated band offsets display excellent agreement with the experiments, demonstrating the validity of the BS MC scheme and the newly developed HSE method. Besides the band offset, the HSE calculated results show similar features (e.g., the band edge wave functions) as the one calculated by the GGA method as discussed above. All the structures tend to have the unified band offset which is unrelated to the thickness of the transition regions. Similar to the GGA calculations, the bulk Si like band edge has been pushed into the SiO_2 region for the structures with "thick" transition regions (such as $n = 4$). Here, we want to emphasize that our HSE method does not need postprocessing corrections to the Si or SiO_2 separately, which provides a consistent description of the charge density, wavefunction and potential of the interface. These quantities can be used for further analysis such as charge transfer crossing the interface. We do note that, in the above, local density of state (LDOS) is used to determine the band offset. This could include the quantum confinement effect due to the small thickness of the c-Si layer. A common way to avoid such quantum confinement effect is to use local potential profile, instead of LDOS. However, the

LDOS determined band gap for the Si region is about 1.1 eV, similar to the result of the HSE bulk Si band gap. This indicates that the quantum confinement effect in this system is relatively small. This is probably because the Si effective masses of both the conduction band in the Γ-X direction, and the valence band heavy-hole, are rather large.

As aforementioned, we also calculate the band offset of the structure prepared by the ReaxFF MD simulation. By taking the snapshots out of the MD trajectory after equilibration, the electronic structure and band offset of the a-SiO2/c-Si interface are calculated using GGA. The direct structure prepare by the MD simulated annealing usually do have one or two defect states due to imperfect bonding topology. However, a small amount of hydrogen atoms can be used to compensate the dangling bonds at those defect sites to eliminate the in-the-gap defect states. The band gap, CBO and VBO are from GGA calculations are 0.76, 2.92 and 2.06 eV, respectively. It is also shown that both the CBM and VBM come from the Si part, which suggests a straddling type of band alignment similar to BS results (Fig. 5). As a summary, Table I summarizes the calculated band offsets from BS MC and ReaxFF MD simulations. Since the GGA calculated ReaxFF CBO is 1 eV higher than the results of BS MC, it indicates that that GGA band corrected band offset would be 1 eV off from that of the experimental results. Such deviation with the ReaxFF MD simulation may arise from the less accurate O–Si–O angle description as well as the dangling bonds emerging during the MD. Although ReaxFF allows ones to simulate the process of bond breaking and bond formation, which is quite relevant for the formation of amorphous structure in this case, the final structure would be subject to how the force fields were trained, typically against DFT-derived energies as well as the simulated annealing procedure. Nevertheless, if an accurate ReaxFF is obtained, and sufficient simulation time is possible, the ReaxFF can be used to simulate the actual synthesis process, which is missing in the BS MC method. In contrary, BS MC using VFF conserves the bonding orders to avoid the dangling bond. Thus by design, the BS MC gives better covalent bonding topology, leading to less defect. This however also lacks some real situations such as the bonding defects in reality. In practice, we found that the BS MC provides better amorphous structure in our calculation.

IV. CONCLUSION

Although the crystalline Si/amorphous SiO_2 is widely used for numerous applications, its band offset dependence on the thickness of the transitional region is not fully explored. In this work, by performing bond switching Monte-Carlo simulation and first-principle calculations, we have

TABLE I. Conduction and valence band offsets (eV) computed by ReaxFF MD, BS MC, and the HSE corrected BS. Other computational work with GGA or LDA and the experimental results are listed for comparison.

	ReaxFF	BS	BS-HSE	Other work (GGA/LDA)	Expt.
Conduction band offset	2.9	1.8	2.9	1.8[7],2.3[52]	3.0[56]
Valence band offset	2.1	2.5	4.4	2.5[7],2.5[52]	4.3[57]

studied the band offset of crystalline Si/amorphous SiO_2 interface under different thickness of the transitional region. For these structures with different thickness, we find that, although the detailed atomic structures near the interface differs significantly, the band offsets of all the different thickness tend to be the same. On the other hand, the bulk Si band edge feature has been extended into the transition area, which leads to a smaller effective SiO_2 region. Our calculation shows that the band offset is rather robust against the details of the transition layers. This is a major advantage for electronic devices, since it can reduce the device variations, a major issue when the device length shrinks to nano size. As a comparison, we also performed reactive force field molecular dynamics simulation to construct the interface. The calculated band offset shows that bond switching method tends to give more consistent results with the experiment, both for the atomic structure and electronic band offset. Moreover, by applying the newly developed hybrid functional with atomic specific mixing parameters, we can correct the band gap of Si and amorphous SiO_2 simultaneously in one heterostructure calculation, thus it can be used for future studies like transports and defect state carrier localizations.

V. ACKNOWLEDGMENT

This material is based on the work performed by the Joint Center for Artificial Photosynthesis, a DOE Energy Innovation Hub, supported through the Office of Science of the U.S. Department of Energy under Award number DE-SC0004993. We use the resource of National Energy Research Scientific Computing center (NERSC) located in Lawrence Berkeley National Laboratory.

[1] S. C. Witczak, J. S. Suehle, and M. Gaitan, Solid-State Electronics **35**, 345 (1992).

[2] A. C. Diebold, D. Venables, Y. Chabal, D. Muller, M. Weldon, and E. Garfunkel, Materials Science in Semiconductor Processing **2**, 103 (1999).

[3] A. Stesmans and V. V. Afanas'ev, Journal of Physics: Condensed Matter **10**, L19 (1998).

[4] Z. H. Lu, M. J. Graham, D. T. Jiang, and K. H. Tan, Applied Physics Letters **63**, 2941 (1993).

[5] D. A. Muller, T. Sorsch, S. Moccio, F. H. Baumann, K. Evans-Lutterodt, and G. Timp, Nature **399**, 758 (1999).

[6] S. Dumpala, S. R. Broderick, U. Khalilov, E. C. Neyts, A. C. T. van Duin, J. Provine, R. T. Howe, and K. Rajan, Applied Physics Letters **106**, 011602 (2015).

[7] F. Giustino, A. Bongiorno, and A. Pasquarello, Journal of Physics: Condensed Matter **17**, S2065 (2005).

[8] S. D. Kosowsky, P. S. Pershan, K. S. Krisch, J. Bevk, M. L. Green, D. Brasen, L. C. Feldman, and P. K. Roy, Applied Physics Letters **70**, 3119 (1997).

[9] F. Giustino and A. Pasquarello, Physical Review Letters **95** (2005), 10.1103/PhysRevLett.95.187402.

[10] T. Watanabe, Japanese Journal of Applied Physics **38**, L366 (1999).

[11] D. Fischer, A. Curioni, S. Billeter, and W. Andreoni, Applied Physics Letters **88**, 012101 (2006).

[12] Z. Huiwen, L. Yongsong, M. Lingfeng, S. Jingqin, Z. Zhiyan, and T. Weihua, Journal of Semiconductors **31**, 082003 (2010).

[13] A. Pasquarello, M. S. Hybertsen, and R. Car, Physical Review Letters **74**, 1024 (1995).

[14] A. Pasquarello, M. S. Hybertsen, and R. Car, Physical Review B **53**, 10942 (1996).

[15] T. Yamasaki, C. Kaneta, T. Uchiyama, T. Uda, and K. Terakura, Physical Review B **63** (2001), 10.1103/PhysRevB.63.115314.

[16] K. Kutsuki, T. Ono, and K. Hirose, Science and Technology of Advanced Materials **8**, 204 (2007).

[17] B. E. Deal and C. R. Helms, *The Physics and Chemistry of SiO2 and the Si-SiO2 Interface* (Springer Science & Business Media, 2013) google-Books-ID: dg73BwAAQBAJ.

[18] P. F. Satterthwaite, A. G. Scheuermann, P. K. Hurley, C. E. D. Chidsey, and P. C. McIntyre, ACS Applied Materials & Interfaces **8**, 13140 (2016).

[19] A. Bongiorno, A. Pasquarello, M. S. Hybertsen, and L. C. Feldman, Physical Review Letters **90** (2003), 10.1103/PhysRevLett.90.186101.

[20] F. Rochet, C. Poncey, G. Dufour, H. Roulet, C. Guillot, and F. Sirotti, Journal of Non-Crystalline Solids Structure and Defects in SiO{in2}, Fundamentals and Applications, **216**, 148 (1997).

[21] F. J. Himpsel, F. R. McFeely, A. Taleb-Ibrahimi, J. A. Yarmoff, and G. Hollinger, Physical Review B **38**, 6084 (1988).

[22] K. Kimura and K. Nakajima, Applied Surface Science Proceedings of the Fourth International Symposium on the Control of Semiconductor Interfaces Karuizawa, Japan, October 21-25, 2002, **216**, 283 (2003).

[23] N. Awaji, Japanese Journal of Applied Physics **35**, L67 (1996).

[24] T. Suwa, A. Teramoto, K. Nagata, A. Ogura, H. Nohira, T. Muro, T. Kinoshita, S. Sugawa, T. Ohmi, and T. Hattori, Microelectronic Engineering Insulating Films on Semiconductors 2013, **109**, 197 (2013).

[25] J. H. Oh, H. W. Yeom, Y. Hagimoto, K. Ono, M. Oshima, N. Hirashita, M. Nywa, A. Toriumi, and A. Kakizaki, Physical Review B **63**, 205310 (2001).

[26] G. Lucovsky and J. C. Phillips, Journal of Physics: Condensed Matter **16**, S5139 (2004).

[27] A. C. T. Van Duin, A. Strachan, S. Stewman, Q. Zhang, X. Xu, and W. A. Goddard, J. Phys. Chem. A **107**, 3803 (2003).

[28] K.-O. Ng and D. Vanderbilt, Physical Review B **59**, 10132 (1999).

[29] S. Lee, R. J. Bondi, and G. S. Hwang, Journal of Applied Physics **109**, 113519 (2011).

[30] S. von Alfthan, A. Kuronen, and K. Kaski, Physical Review B **68** (2003), 10.1103/PhysRevB.68.073203.

[31] T. Anh Pham, T. Li, H.-V. Nguyen, S. Shankar, F. Gygi, and G. Galli, Applied Physics Letters **102**, 241603 (2013).

[32] A. Alkauskas, P. Broqvist, F. Devynck, and A. Pasquarello, Phys. Rev. Lett. **101**, 106802 1 (2008).

[33] B. R. Tuttle, Physical Review B **70** (2004), 10.1103/PhysRevB.70.125322.

[34] Y. Tu, J. Tersoff, G. Grinstein, and D. Vanderbilt, Physical Review Letters **81**, 4899 (1998).

[35] H. H. Pham, G. T. Barkema, and L.-W. Wang, Physical Chemistry Chemical Physics **17**, 26270 (2015).

[36] N. Mousseau and G. T. Barkema, Journal of Physics: Condensed Matter **16**, S5183 (2004).

[37] L. Kong and L. J. Lewis, Physical Review B **77**, 085204 (2008).

[38] J. Tersoff, Physical Review B **38**, 9902 (1988).

[39] J. Tersoff, Physical Review B **39**, 5566 (1989).

[40] S. R. Billeter, A. Curioni, D. Fischer, and W. Andreoni, Physical Review B **73**, 155329 (2006).

[41] J. Yu, S. B. Sinnott, and S. R. Phillpot, Physical Review B **75**, 085311 (2007).

[42] A. Yasukawa, JSME international journal. Ser. A, Mechanics and material engineering **39**, 313 (1996).

[43] T. Watanabe, H. Fujiwara, H. Noguchi, T. Hoshino, and I. Ohdomari, Japanese Journal of Applied Physics **38**, L366 (1999).

[44] Y. Tu and J. Tersoff, Physical Review Letters **84**, 4393 (2000).

[45] A. C. T. van Duin, A. Strachan, S. Stewman, Q. Zhang, X. Xu, and W. A. Goddard, The Journal of Physical Chemistry A **107**, 3803 (2003).

[46] G. Kovacevic and B. Pivac, Journal of Applied Physics **115**, 043531 (2014).

[47] W. Jia, Z. Cao, L. Wang, J. Fu, X. Chi, W. Gao, and L.-W. Wang, Computer Physics Communications **184**, 9 (2013).

[48] W. Jia, J. Fu, Z. Cao, L. Wang, X. Chi, W. Gao, and L.-W. Wang, Journal of Computational Physics **251**, 102 (2013).

[49] J. P. Perdew, K. Burke, and M. Ernzerhof, Phys. Rev. Lett. **77**, 3865 (1996).

[50] P. Giannozzi, S. Baroni, N. Bonini, M. Calandra, R. Car, C. Cavazzoni, D. Ceresoli, G. L. Chiarotti, M. Cococcioni, I. Dabo, A. D. Corso, S. de Gironcoli, S. Fabris, G. Fratesi, R. Gebauer, U. Gerstmann, C. Gougoussis, A. Kokalj, M. Lazzeri, L. Martin-Samos, N. Marzari, F. Mauri, R. Mazzarello, S. Paolini, A. Pasquarello, L. Paulatto, C. Sbraccia, S. Scandolo, G. Sclauzero, A. P. Seitsonen, A. Smogunov, P. Umari, and R. M. Wentzcovitch, J. Phys.: Condens. Matter **21**, 395502 (2009).

[51] D. R. Hamann, Physical Review B **88**, 085117 (2013).

[52] A. Alkauskas, P. Broqvist, F. Devynck, and A. Pasquarello, Physical Review Letters **101** (2008), 10.1103/PhysRevLett.101.106802.

[53] J. H. Skone, M. Govoni, and G. Galli, Physical Review B **89** (2014), 10.1103/PhysRevB.89.195112.

[54] S. Susman, K. J. Volin, D. L. Price, M. Grimsditch, J. P. Rino, R. K. Kalia, P. Vashishta, G. Gwanmesia, Y. Wang, and R. C. Liebermann, Physical Review B **43**, 1194 (1991).

[55] K. Laaziri, S. Kycia, S. Roorda, M. Chicoine, J. L. Robertson, J. Wang, and S. C. Moss, Physical Review B **60**, 13520 (1999).

[56] V. V. Afanas'ev, M. Houssa, A. Stesmans, and M. M. Heyns, Applied Physics Letters **78**, 3073 (2001).

[57] J. W. Keister, J. E. Rowe, J. J. Kolodziej, H. Niimi, T. E. Madey, and G. Lucovsky, Journal of Vacuum Science & Technology B: Microelectronics and Nanometer Structures Processing, Measurement, and Phenomena **17**, 1831 (1999).

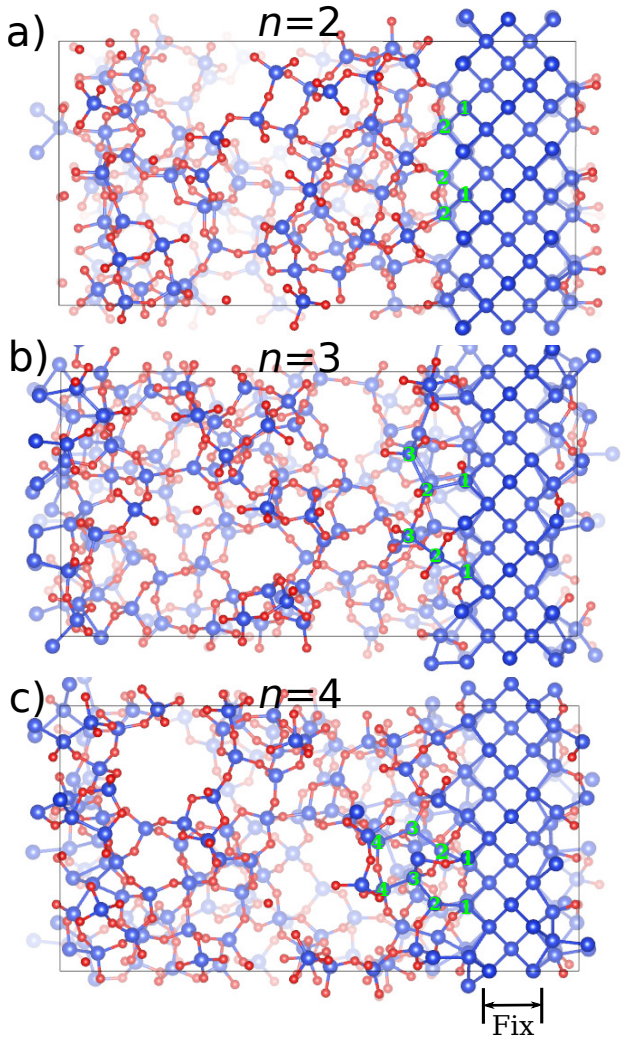

FIG. 1. The DFT relaxed structures taking from the MC simulations. Here, different maximum number of Si atoms (n) connected via the continued Si–Si bonds are used to represent the thickness of the transition region. a) $n = 2$, b) $n = 3$, and c) $n = 4$. The green digits are used to count the Si atoms which are connected by continued Si–Si bonds spreading from the fixed Si atoms as examples. The middle three Si layer are fixed in MC simulation and DFT relaxation. The Si–Si bonds connected to these fixed atoms are not allowed to switch during the MC simulation.

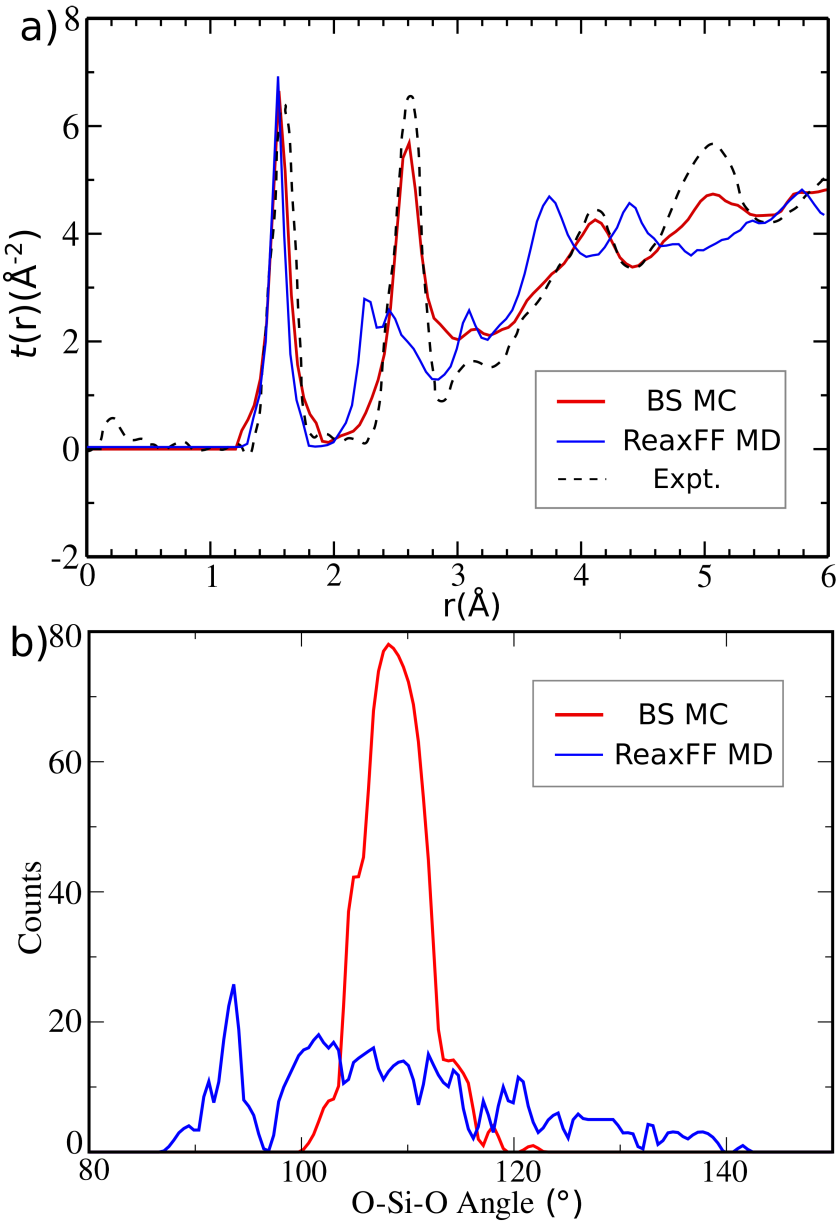

FIG. 2. a) Radial distribution function (RDF) comparison from BS MC, ReaxFF MD and experimental values. b) O–Si–O angle distribution histogram of the structures from BS MC and ReaxFF MD.

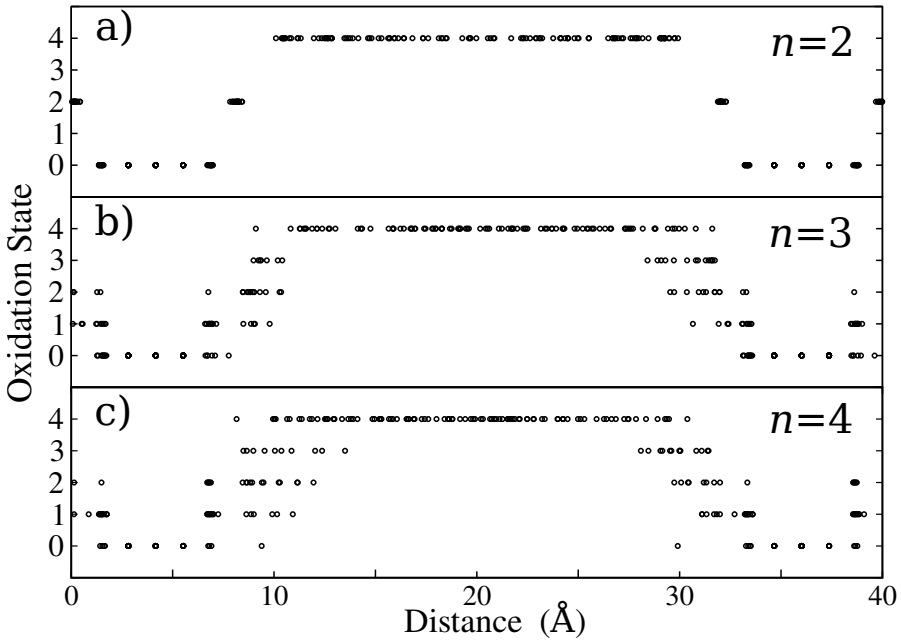

FIG. 3. The oxidation states of Si atoms averaged for a given distance along [001] direction for the whole supercell under different n.

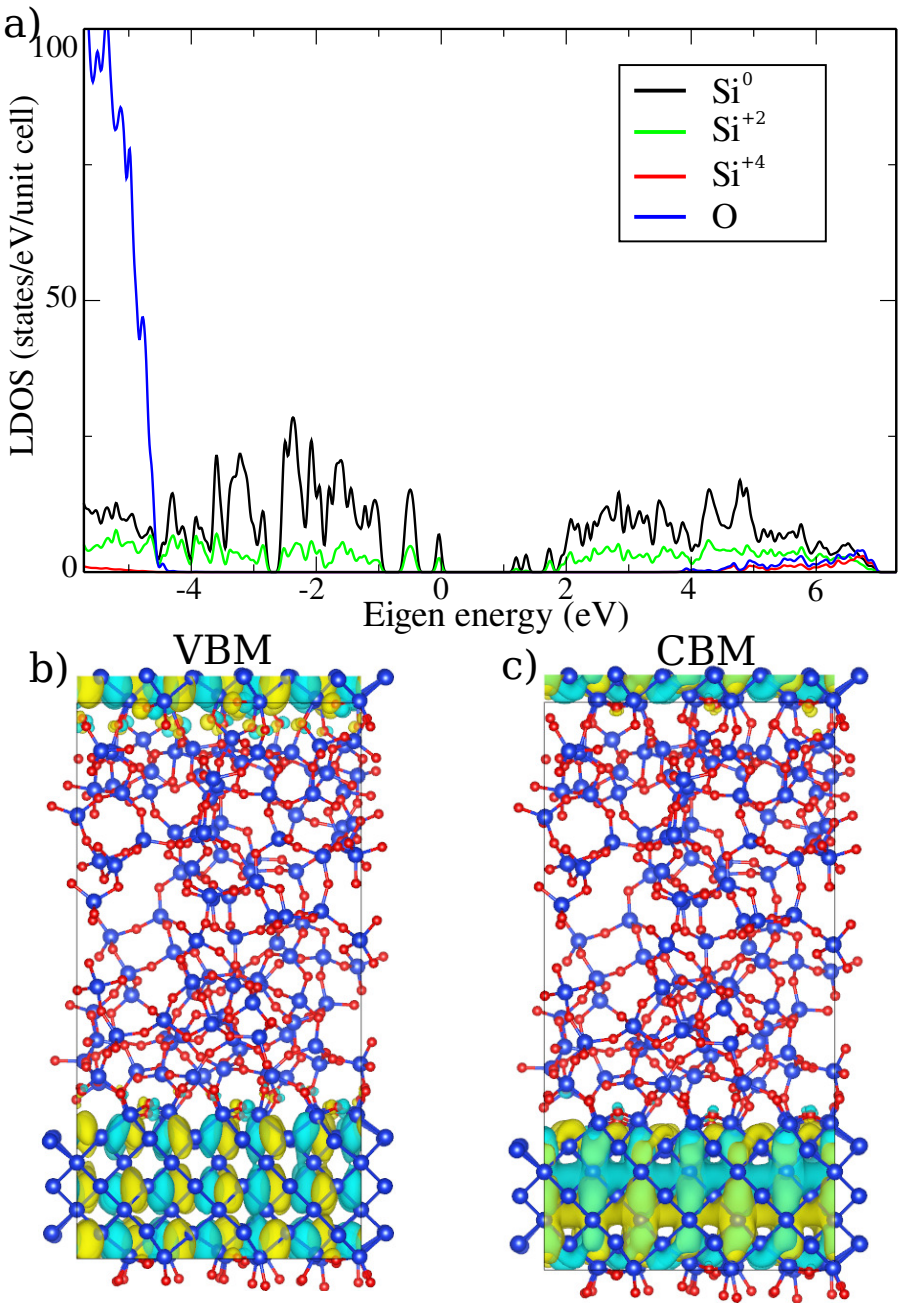

FIG. 4. a) The HSE calculated local density of states for Si^0 atoms (Si-bulk part), Si^{+2} (transition region), Si^{+4} (SiO_2-bulk part) and O (SiO_2-bulk part) atoms obtained from the n=2 structure. Here, the Si^{+4} and O atoms are from the middle of the SiO_2-bulk part to exclude the contribution from interfacial region. 0 energy is set to be at the valence band minimum. Real space wavefunction isosurface for the b) valence band maximum (VBM), and c) conduction band minimum (CBM) of this structure.

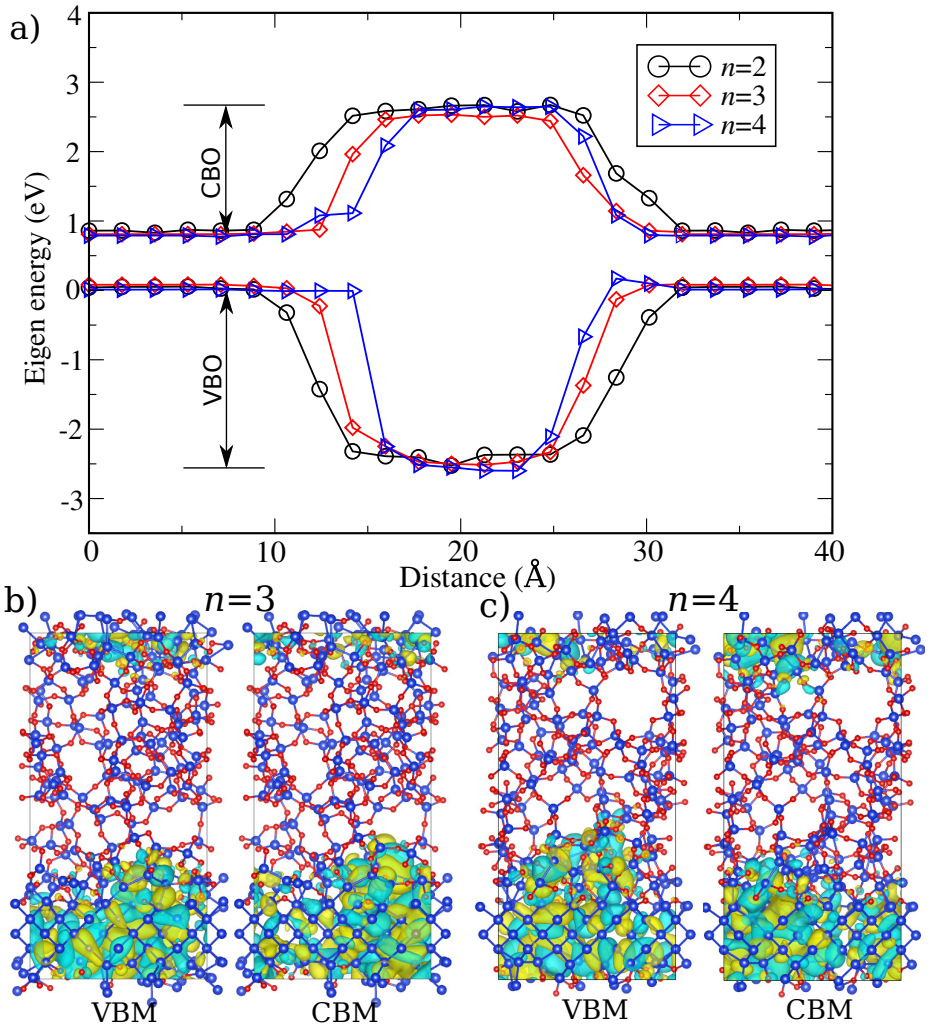

FIG. 5. a) The GGA calculated VBM and CBM averaged for a given distance along [001] direction across the interface for structures with n=2, 3 and 4. Left and right ends correspond to the Si-bulk part, with 0.8 eV band gap; the middle part corresponds to the SiO_2-bulk part, with around 5.2 eV band gap. The valence band offset is computed as 2.5 eV, and the conduction is 1.8 eV. b) The VBM and CBM wavefunctions in real space for the structures with n=3 and 4.

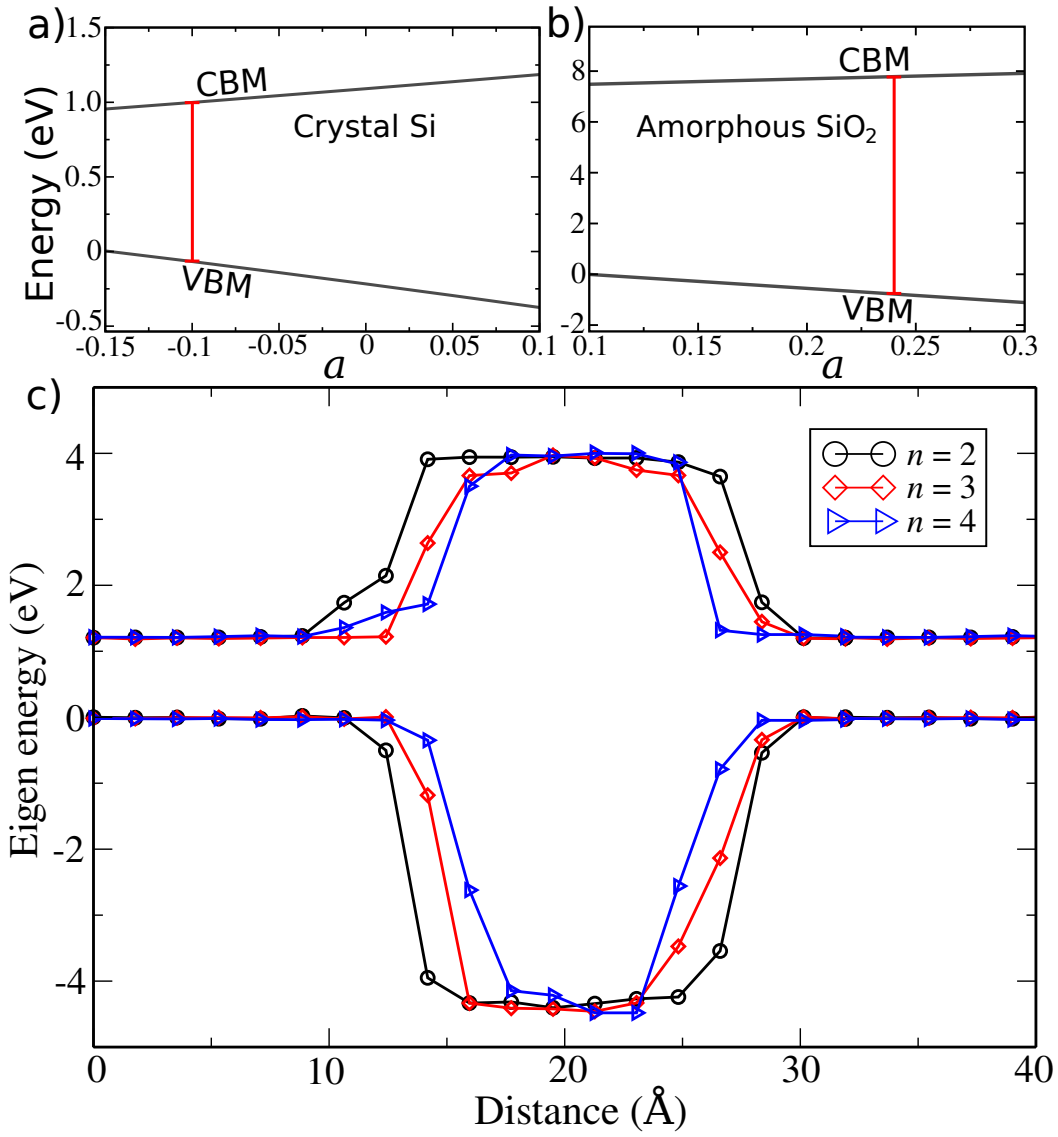

FIG. 6. a) CBM and VBM energy of silicon crystal calculated by different mixing parameter α of HSE. Here, α is adjusted by a as described in Methods. b) VBM and VBM energy of the 243-atom amorphous SiO_2 with different α. c) HSE calculated band offset of the structure for the structures with n=2, 3 and 4.